Polymorphism of a Lipid Extract from *Pseudomonas fluorescens*: Structure Analysis of a Hexagonal Phase and of a Novel Cubic Phase of Extinction Symbol *Fd*--†

Paolo Mariani,‡ Emilio Rivas,§ Vittorio Luzzati,*,∥ and Hervé Delacroix∥

Istituto di Fisica Medica, Università di Ancona, Via Monte d'Ago, 60100 Ancona, Italy, Centre Réactionnel Photosynthétique, CNRS, 91198 Gif-sur-Yvette, France, Instituto de Biologia Celular, CONICET, Buenos Aires, Argentina, and Centre de Génétique Moléculaire, Laboratoire Propre du CNRS Associé à l'Université Pierre et Marie Curie, 91198 Gif-sur-Yvette, France

Received December 5, 1989; Revised Manuscript Received February 15, 1990

ABSTRACT: The phase diagram of the *Pseudomonas fluorescens* lipid extract is unusual, in the sense that it displays a cubic phase straddled by a hexagonal phase. The hexagonal phase was studied over an extended concentration range, and the reflections were phased on the assumption that the structure contains circular cylinders of known radius. The cubic phase, whose extinction symbol is *Fd*--, was analyzed by reference to space group No. 227 (*Fd*3*m*). The phases of the reflections were determined by using a novel pattern recognition approach, based upon the notion that the average fourth power of the electron density contrast $\langle(\Delta r)^4\rangle$ is dependent on chemical composition but not on physical structure, provided that the function $\Delta r(\mathbf{r})$ satisfies the constraints $\langle(\Delta r)\rangle = 0$ and $\langle(\Delta r)^2\rangle = 1$. As a further constraint, a shape normalization is used, in the form of a Gaussian apodization of the intensities, which has the effect of normalizing the curvature of the autocorrelation function at the origin. We analyzed two cubic samples of different composition: for each of them we generated all the phase combinations compatible with the X-ray scattering data and we searched for those whose $\langle(\Delta r)^4\rangle$ best agrees with the hexagonal phase. Taking advantage of the favorable properties of the phase diagram, we carefully explored the effects of various parameters; we concluded that the chemical composition of the phases being compared must be identical, that the X-ray scattering data should not be truncated artificially, and that the apodization must be mild so that the curvature takes a value intermediate between those corresponding to the raw data of the two phases. When all these precautions were taken, $\langle(\Delta r)^4\rangle$ was found to be remarkably invariant; this conclusion is important in view of the possible usefulness of the novel technique in tackling ab initio—and at very low resolution—structural problems of more general interest. The structure of the cubic phase consists of a 3D network of rods joined tetrahedrally 4 by 4 according to a diamond lattice and of a family of quasi-spherical disjointed micelles; the core of the rods and of the micelles is polar, and the interstices are filled by the hydrocarbon chains (structure of type II). All the dimensions (diameter of rods and micelles, area per chain at the polar/apolar interface) are consistent with the chemical properties of the system. The structure—which is bicontinuous like that of most of the cubic phases—may be visualized as a 3D generalization of the *lipid monolayer*. The structure, moreover, does *not* belong to the class of the infinite periodic surfaces without intersections.

Lipid polymorphism is a fascinating phenomenon: no other class of chemical compounds is known to display such a variety of structures over such a narrow range of physical and chemical parameters, and so close to physiological conditions. Soon after the phenomenon was discovered, some authors suggested that similar polymorphic transitions may occur in the lipid moiety of biological membranes and thus play a physiological role; this hypothesis has been with us for some 30 years but is still wanting for convincing experimental support [see, for the early work, Luzzati and Husson (1962), Luzzati (1968), Shipley (1973), Luzzati (1981), and Luzzati et al. (1986); see Seddon (1989) for a review of the more recent work].

Since the early days of lipid polymorphism, one class of phases caught the observers' attention: these phases are optically isotropic and highly viscous, their NMR signals are as sharp as those of the dilute micellar solution (by contrast, the NMR signals of the other liquid-crystalline phases are broad), and the X-ray scattering spectra consist of sharp small-angle reflections and of a broad (4.6 $Å^{-1}$) band characteristic of liquid paraffins. The organization of these phases was soon shown to belong to the liquid-crystalline class and to display cubic symmetry; for some time, though, their structures remained elusive. Eventually, the structure of one of those phases was solved (Luzzati & Spegt, 1967); further, as a result of a systematic search of lipid-containing systems, Tardieu (1972) reported five different cubic phases, identified the extinctions symbol of four and proposed structures for two [besides the one reported by Luzzati and Spegt (1967)]. Several structures have been put forward since, but most proposals have lacked unequivocal experimental support [reviewed by Mariani et al. (1988)].

Around 1986 we felt it timely to investigate the whole problem of the structure of the cubic phases; for that purpose we undertook a mathematical analysis of ab initio crystallographic structure determinations at very low resolution. The spirit of our approach was to generate first all the phase combinations (the φ-sets) compatible with the observed re-

† This work was supported in part by grants from the Association Française pour la Recherche Médicale and from the Ligue Nationale Française centre le Cancer. P.M. acknowledges the financial support of the Commission of the European Community (Stimulation Plan) and of the European Molecular Biology Organization.

* To whom correspondence should be addressed.
‡ Università di Ancona.
§ CNRS and CONICET.
∥ Centre de Génétique Moléculaire, CNRS.

0006-2960/90/0429-6799$02.50/0

flections and then to screen them according to mathematical criteria based upon the chemical properties of the system. The basic assumption underlying our analysis was that the histogram of the electron density maps—properly normalized in scale and shape—is strongly dependent upon chemical composition, but almost independent of the precise space distribution of scattering matter. Therefore, it was our contention that, for any pair of phases with the same chemical composition, the φ-sets associated with the observed structure factors should be related by strict mathematical rules: in other words, the structure of one of the phases can be used to determine the structure of the other. We worked out an algorithm that we applied to the six known types of cubic phases (Mariani et al., 1988): for the two phases whose structure was known (Q^{230} and Q^{224}), the results were in perfect agreement with those structures; for three unknown phases (Q^{229}, Q^{212}, Q^{227}), novel structures were obtained that agree with the chemical properties of the system; for one phase (Q^{223}), the analysis led to controversial results.

One of the cubic phases (extinction symbol *Fd--*) had been discovered by Tardieu (1972), using a lipid preparation from *Pseudomonas fluorescens* provided by E. Rivas. Lack of reproducibility, due apparently to uncontrolled parameter(s) in the chemical purification, prevented a proper analysis (and publication) of that early observation. More recently, phases with the same symmetry have been observed in other lipid preparations: mixtures of monoolein and oleic acid in excess water at acidic pH (Mariani et al., 1988), oleic acid in excess water at slightly acidic pH (J. Seddon, private communication), and some ill-defined commercial cosmetic preparations (T. Gulik, private communication). Besides, a cubic phase reported by Das and Rand (1986) in the system diacylglycerol–egg phosphatidylcholine–water also seems to belong to space group *Fd3m*, with $a = 133$ Å, according to the spacing and intensity of the reflections (see Table II of that paper). Assuming that all those phases have the same structure, we concluded from our analysis that all contain a 3D network of rods, tetrahedrally joined 4 by 4 and organized in a diamond lattice, and a system of disjointed micelles (Mariani et al., 1988).

The unusual phase diagram of *P. fluorescens* lipids—a cubic phase is observed, straddled by a hexagonal phase (Figure 1)—and the novelty of a structure containing both rods and micelles prompted us to carry out a proper chemical characterization of the lipid extract and to perform a careful crystallographic analysis of both the hexagonal and the cubic phases. Our purpose was multifold: to critically scrutinize the arguments in support of the structures of the cubic phases; to carefully analyze the structure of the hexagonal phase (2D electron density maps are rare in lipid literature, by contrast with the 1D maps of the lamellar phases); to cautiously explore the idiosynchrasy of the phasing algorithm, taking full advantage of the unusual and highly favorable features of the phase diagram.

Materials and Methods

(*a*) *Lipid Extraction.* The bacterium *P. fluorescens*, strain ATCL 17823, was grown in (stirred) PAB liquid culture medium at 15 °C for approximately 28 h. After centrifugation, the lipids were extracted from the pellet by using a technique derived from Nichols (1963), as described by Rivas and Luzzati (1969). A first extraction was carried out with 2-propanol, under conditions in which the lipase activity is negligible (Kates, 1960) (apparently, this is an important precaution in order to obtain a lipid extract whose properties are those described in this work). The residue was subsequently extracted with chloroform–methanol (1:1 v/v). The solvents were removed by evaporation at low temperature. The final extraction was performed with chloroform–methanol (2:1 v/v) and the solution purified by the method described by Folch et al. (1957). Freshly extracted and dried lipids were used for the chemical analyses.

(*b*) *Chemical Analyses.* Silicic acid (Mallincrodt, St. Louis, MO) was used for the fractionation of the lipid extract. Neutral lipids were eluted with chloroform and polar lipids with methanol; the two fractions were dried in vacuo and weighed.

Individual lipid species were separated by thin-layer chromatography. Neutral lipids were resolved on silica gel G plates in petroleum ether–diethyl ether–acetic acid (80:20:2 volume ratios). Chloroform–methanol–acetic acid (65:24:2 volume ratios) was used to resolve the phospholipids.

A solution of 0.2% anthrone in concentrated sulfuric acid was used to distinguish glycolipids from other lipid-soluble components. Molybdenum blue reagent (Varskovsky & Kostetsky, 1968) was used to locate phospholipids. Lipid phosphorus was determined quantitatively in the TLC spots scraped from the plates according to Rouser et al. (1970). Neutral and polar lipids were quantified after the chromatographic separation by charring with cupric acetate–phosphoric acid reagent (Macala et al., 1983) and densitometry.

Proteins were determined according to Lowry et al. (1951), using bovine serum albumin as the standard.

(*c*) *X-ray Diffraction.* The samples were prepared by mixing controlled amounts of dried lipids and distilled water and keeping the mixture at room temperature until equilibrium was reached (usually in a few days). Thereafter, the X-ray scattering spectra were tested to be time independent for periods of several weeks and to be invariant through cycles of thermal treatment or of water removal and addition. The X-ray scattering experiments were performed by using a sealed microfocus tube and a temperature-controlled Guinier camera, operating in vacuo. A bent quartz monochromator focused the X-ray beam and isolated the Cu $K\alpha_1$ line. The samples were held in vacuum-tight cylindrical cells with thin mica windows. The cells were rotated continuously during the exposure in order to reduce the spottiness arising from the macroscopic monodomains. The temperature was controlled within approximately 0.5 °C. The intensity of the reflections was measured with a Joyce-loebl microdensitometer (Model MKII CS) and corrected as described elsewhere [see Tardieu (1972) for a more detailed technical description].

(*d*) *Notation.* $\mathbf{r}$ (in Å) and $\mathbf{s}$ (in Å^{-1}): vectors specifying the position in real and in reciprocal spece; r and s are the moduli; $s = (2 \sin \theta)/\lambda$; 2θ is the scattering angle and λ the wavelength.

$\mathbf{s_h}$ ($\mathbf{h} = \{hkl\}$): vector specifying the position of the reciprocal lattice points.

$\langle g \rangle$: average value of a periodic function $g(\mathbf{r})$ over the volume V of the unit cell; $\langle g \rangle = (1/V)\int_V g(\mathbf{r})\, dv_\mathbf{r}$.

$\mathbf{F(h)} = \int_V \rho(\mathbf{r}) \exp(-2\pi i \mathbf{r}\cdot\mathbf{s_h}) dv_\mathbf{r}$: structure factor; $F(\mathbf{h})$ and $\varphi(\mathbf{h})$ are its modulus and phase.

$\rho(\mathbf{r})$: Fourier transform of $\mathbf{F(h)}$.

$\Delta\rho(\mathbf{r}) = [\rho(\mathbf{r}) - \langle\rho\rangle][\langle\rho^2(\mathbf{r})\rangle - \langle\rho\rangle^2]^{-1/2}$: normalized dimensionless expression of the function $\rho(\mathbf{r})$, also called the map.

V: volume of the 1D, 2D, or 3D unit cell.

$p(r) = (2/r)\int si(s) \sin 2\pi rs\, ds$: spherical average of the autocorrelation function of $\Delta\rho(\mathbf{r})$; $i(s)$ is the spherical average of $|\mathbf{F(h)}|^2$.

φ-set: set of phase angles associated with the structure factors of the observed reflections.

Table I: Chemical Composition of the Lipid Extract[a]

component[b]	Ψ (%)	$\bar{v}$ (cm^3/g)	$\langle MW \rangle$	$\langle MW \rangle_{pol}$	v_{mol} (Å^3)	v_{pol} (Å^3)	footnote
PE	47.7	1.006	704.2	270.2	1176.4	282.2	*c*
PG	9.8	0.983	734.2	300.2	1199.0	304.8	*d*
CL	9.0	1.006	1376.3	508.3	2299.2	510.7	*c*
GL	3.0	0.983	814.0	381.6	1329.3	435.1	*e*
dG	1.4	1.090	580.1	146.1	1050.2	157.0	*f*
FA	11.9	1.152	262.0	45.1	501.6	54.5	*g*
tG	0.8	1.154	824.1	0	1579.8	0	*h*
HC	13.1	1.200	248.1	0	494.6	0	*i*
proteins	2.4						
unidentified	0.8						

[a] Ψ is the weight percent of the lipid component, $\bar{v}$ is the partial specific volume, $\langle MW \rangle$ and $\langle MW \rangle_{pol}$ are the (molecular) weights of the average molecule and of its polar moiety, and v_{mol} and v_{pol} are the volumes of the average molecule and of its polar moiety. Volumes are all reduced to 60 °C [$V_{t+\Delta t} = V_t(1 + 7.48 \times 10^{-4}\Delta t)$; Tardieu, 1972]. At 60 °C, the volumes occupied by the CH, CH_2, and CH_3 groups are respectively 21.0, 27.7, and 55.4 Å^3 (Tardieu, 1972). [b] Abbreviations: PE, phosphatidylethanolamine; dG, diglycerides; FA, fatty acids; tG, triglycerides; HC, hydrocarbons. [c] Gulik-Krzywicki et al. (1967). [d] Rivas and Luzzati (1969). [e] $\bar{v}$ and $\langle MW \rangle$ estimated from the data of Rivas and Luzzati (1969). [f] $\bar{v}$ estimated from monoglyceride data (Larsson, 1968). [g] $\bar{v}$ estimated from oleic acid (Small, 1986, page 256). [h] $\bar{v}$ and v_{mol} estimated from tripalmitin (Small, 1986, page 367). [i] $\bar{v}$ and v_{mol} estimated from long-chain alcohols and esters (Small, 1986, page 233).

rank γ: absolute position of one particular φ-set in the list of all the Γ possible φ-sets, sorted in the order of increasing $\langle(\Delta\rho)^4\rangle$.

L and H: 1D lamellar phase and 2D hexagonal phase (space group *p*6).

Q_t: cubic phase of aspect *t* (*International Tables*, 1952, Vol. II, page 147).

Q^m: cubic phase of space group No. *m* (according to the *International Tables*, 1952, Vol. I).

c, c_v: weight and volume concentrations [solute/(solute + solvent)].

$c_{v,par}$: volume concentration of the apolar moiety.

S_{ch}: area per chain at the polar/apolar interface.

(*e*) *Crystallographic Structure Analysis.* The techniques used in the structure analyses of lipid phases generally are restricted to swelling and trial-and-error procedures. Swelling methods have often been applied to lamellar and, more rarely, hexagonal phases; we discuss under Results, section c, a procedure that belongs to that category. Trial-and-error methods may provide powerful tools, especially when the crystallographic and the chemical data are extensive and accurate and when the structure can be reduced to simple models depending on a small number of parameters [reviewed by Mariani et al. (1988)]. Yet, lipid phases do not always display extensive swelling, nor is their structure sufficiently simple to yield to a trial-and-error approach. For these reasons, we have recently tackled the more general problem of structure analyses at very low resolution: we have put forward a novel phasing technique based upon the knowledge of the chemical composition, unit cell dimensions, and space group and involving the intensity of all the reflections within a sphere of radius S_{max} in reciprocal space (Luzzati et al., 1988; Mariani et al., 1988).

Our procedure can be decomposed into a number of steps: (a) shape normalization of the electron density profile, involving a Gaussian apodization of the observed intensities

$$|\mathbf{F}_\beta(\mathbf{h})|^2 = |\mathbf{F}(\mathbf{h})|^2 \exp(-2\beta^2 s_r^2) \quad (1)$$

aimed at adjusting the curvature of the autocorrelation function $p_\beta(r)$ at the point $r = 0$

$$p_\beta''(0) = -(4/3)\pi^2[\textstyle\sum_{\mathbf{h}} s_{\mathbf{h}}^2 |\mathbf{F}_\beta(\mathbf{h})|^2] / [\textstyle\sum_{\mathbf{h}} |\mathbf{F}_\beta(\mathbf{h})|^2] \quad (2)$$

to some preimposed values; (b) scale normalization, achieved by setting the sum of the observed intensities equal to 1

$$\textstyle\sum_{\mathbf{h}} |\mathbf{F}_\beta(\mathbf{h})|^2 = \langle(\Delta\rho)^2\rangle = 1 \quad (3)$$

(c) generation of all the φ-sets consistent with the data and with the two normalizations (note that the phases of a few selected reflections should be fixed beforehand in order to eliminate the redundancies associated with the arbitrary choice of the origin of the cell and of the sign of the electron density contrast); and (d) screening the φ-sets and selecting the "best" one. We have proposed two criteria for that purpose. One resorts to the histogram $\mathbb{H}(\Delta\rho)$ of the map $\Delta\rho(\mathbf{r})$, or, more simply, to its moments $\langle(\Delta\rho)^n\rangle$:

$$\langle(\Delta\rho)^n\rangle = \int_{-\infty}^{\infty} (\Delta\rho)^n \mathbb{H}(\Delta\rho)\, d(\Delta\rho) = (1/V)\int_V [\Delta\rho(\mathbf{r})]^n\, dv_r \quad (4)$$

which, we conjecture, are more specifically dependent on the chemical composition of the phase than on its physical structure. Noting, moreover, that $\langle(\Delta\rho)\rangle$ [$=F(0)$] = 0, that $\langle(\Delta\rho)^2\rangle = 1$ (see eq 3), and that the odd moments of $\Delta\rho$ are poorly selective, we have surmised on theoretical grounds—and amply documented by practical examples—that the parameter $\langle(\Delta\rho)^4\rangle$ is likely to take the same (or very close) value(s) in phases with different structure, provided the chemical composition is the same [and with the reservation that s_{max} and $p_\beta''(0)$ are invariant]. The other criterion, equivalent to a test of smoothness (and also of maximal entropy), is to presume that the "best" φ-set is the one whose $\langle(\Delta\rho)^4\rangle$ is minimum; we have shown that this criterion is satisfactorily fulfilled whenever the map does not depart too strongly from a two-level step function and the volumes of the two steps are approximately equal.

Results

(*a*) *Chemical Data.* The chemical composition of the lipid extract is reported in Tables I and II. The fatty acid composition was taken from Gill (1975): (C16:0)/(C16:1)/(C18:1) = 0.229/0.498/0.272 (weight ratios). The elemental composition of the average fatty acid molecule is $C_{16,15}H_{31,48}O_{2,00}$, its MW is 262.0 and the volume of the hydrocarbon moiety v_{par} = 447.0 Å^3 (at 60 °C).

If the concentration, the partial specific volume, and the elemental composition of the lipid components are taken into account and if the separation between the polar and the apolar regions is set in the middle of the C_α–C_β bond, then it is possible to determine the volume and number of electrons of the polar and of the apolar regions and also to estimate the number of hydrocarbon chains per average lipid molecule. With regard to the partition of the free fatty acids, and in agreement with Gulik et al. (1985), we consider two alternative situations: in one (case A) the headgroups segregate in the core of the apolar regions and in the other (case B) at the

Table II: Paraffin and Molar Moieties[a]

		C	H	O	P	N	MW	n	v	μ
case A	par	24.86	48.83	0.84	0	0	361.3	204.7	728.3	1.014
	pol	3.74	6.35	4.30	0.49	0.35	140.1	72.9	145.7	
case B	par	24.56	48.52	0.30	0	0	348.8	198.3	713.5	1.275
	pol	4.04	6.67	4.83	0.49	0.35	152.6	79.3	160.6	
av lipid molecule							501.3	277.6	874.0	
water	pol	0	2	1	0	0	18.02	10	30.4	

[a] The two paritions (cases A and B) of the polar and the apolar moieties are discussed under Results, section a. In each row, C, H, etc. are the number of oxygen, hydrogen, etc. atoms, MW is the molecular weight, n is the number of electrons, v in the volume of the paraffin and the polar moieties of either an average lipid or a water molecule, and μ is the number of hydrocarbon chains per average lipid molecule (all volumes at 60 °C).

polar/apolar interface. The choice will be discussed under Results, section c.

(*b*) *Phase Diagram.* We have explored the portion of the isobaric temperature–composition phase diagram represented in Figure 1. We have observed four different phases, three of which are characterized by a family of sharp small-angle reflections whose spacings ratios are as follows: L, 1:2:3; H, 1:√3:2:√7:3:√12:√13; Q_{15}, √3:√8:√11:√12:4:√19:√24:√27:.... The presence of a diffuse band centered at 4.6 $Å^{-1}$ indicates that the short-range conformation of the hydrocarbon chains is liquidlike (type α; Luzzati, 1968) in the three phases. We have sketched in Figure 1 the position of the one-phase regions in the phase diagram. We have focused our work on the phases H and Q_{15}, at 60 °C and as a function of concentration.

The presence of a cubic phase straddled by a hexagonal phase (Figure 1) is unusual in lipids: another example is phase Q^{230} of the lipid extract GDNT of *Sulfolobus solfataricus* [see Figure 5 in Gulik et al. (1985)].

(*c*) *Hexagonal Phase.* Hexagonal phases, commonly observed in lipid systems, can be visualized as 2D hexagonal arrays of cylindrical rods, lined by the polar headgroups and embedded in a continuous matrix. Two kinds of distributions of the polar and the apolar moieties must be distinguished: type I, oil in water, when the rods are filled by the hydrocarbon chains and the outer medium is polar; type II, water in oil, in the opposite situation [reviewed by Luzzati (1968)].

An analysis of the dimensions of the structure elements as a function of concentration can discriminate between the two types of structure. Knowing the concentration c and the cell parameter a, and assuming that the rods take the form of circular cylinders, the radius R and the area per chain at the polar/apolar interface S_{ch} can be determined for the two types of structures and for the two definitions of the polar and the paraffin moieties (cases A and B above). The equations involved are

$$(R_{par})_{type\ I} = 0.525a(c_{v,par})^{1/2} \quad (5)$$

$$(S_{ch})_{type\ I} = 3.809v_{par}(\mu a)^{-1}(c_{v,par})^{-1/2} \quad (6)$$

$$(R_{pol})_{type\ II} = 0.525a(c_{v,pol})^{1/2} \quad (7)$$

$$(S_{ch})_{type\ II} = 3.809v_{par}(c_{v,pol})^{1/2}(\mu a c_{v,par})^{-1} \quad (8)$$

$$c_{v,par} = (c_e v_{par}/n_{lip})[c_e v_{lip}/n_{lip} + (1 - c_e)v_{water}/n_{water}]^{-1} \quad (9)$$

$$c_{v,pol} + c_{v,par} = 1 \quad (10)$$

c_e is the electron concentration, in this case barely different from c. The other parameters are defined and their values reported in Tables II and III. The results of applying eqs 5–10 to the data are reported in Table III and plotted in Figure 2. The most striking feature is the trend of the function S_{ch} vs c: if the structure is supposed to be of type II, then S_{ch} increases with increasing c, whereas the opposite occurs if the structure is of type I. It is generally agreed that, at constant temperature, the parameter S_{ch} increases—or at least does not decrease—as the water content increases; on this ground we conclude that the structure of phase H is of type II. This conclusion is confirmed by the observations that if the structure is of type II, then the values of S_{ch} are in excellent agreement with those of other lipids and no point in the hydrocarbon region is further away from the polar/apolar interface than the fully extended length of the hydrocarbon chains (approximately 18 Å, to be compared with the parameter d of Table III). On the contrary, both S_{ch} and the radius of the cylinders would be too large if the structure were of type I.

Regarding the discrimination between cases A and B, the values of S_{ch} (see Figure 2) are in slightly better agreement with those of other lipids for case B than for case A. We henceforth assume that the headgroups of the free fatty acids

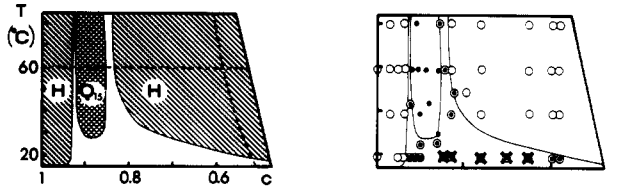

FIGURE 1: Schematic representation of the isobaric- (T, c) dependent phase diagram of the lipid extract. c is the weight concentration. (Right frame) Position of the experimental points: (●) phase Q^{227}; (○) phase H; (open dotted circle) phases Q^{227} and H; (closed crossed circle) phases Q^{227}, H, and L. (Left frame) One-phase domains: H, hatched; Q^{227}, crosshatched. The samples studied in this work (see Tables III and IV) lie on the 60 °C line.

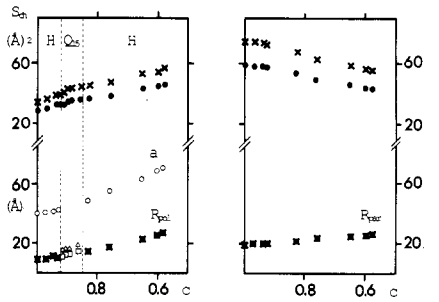

FIGURE 2: Dimensions of the structure elements as a function of concentration. a is the parameter of the 2D hexagonal cell, S_{ch} is the area per chain at the polar/apolar interface. (Left frame) Structure of type II (water in oil); R_{pol} is the radius of the polar cylinder. (Right frame) Structure of type I (oil in water); R_{par} is the radius of the hydrocarbon cylinder. Cases A (×) and B (●) refer to different partitions of the headgroups of the fatty acids between the polar and the apolar moieties (see text). With regard to the cubic phase, the partition of the apolar (typ I) or the polar (type II) volumes between the rods and the spheres is such that the parameter S_{ch} takes the same value in the two types of structure elements (see text). In the left lower frame (corresponding to type II, case B), the points △ and □ mark the radius of the spherical and the rodlike structure elements, respectively. Phase Q_{15} is omitted in the right frame.

Table III: Parameters of the Hexagonal Phase[a]

						interpolated					
c	0.58	0.60	0.65	0.76	0.83	0.86	0.91	0.93	0.94	0.97	1.00
a (Å)	69.7	68.2	62.9	54.4	48.2	45.5	43.0	42.3	41.5	40.7	39.8
$F(10)$	284	294	320	384	399	401	402	402	403	404	398
$F(21)$	−212	−205	−182	−81	−34	−29	45	52	53	56	76
$F(20)$	−183	−180	−165	−97	−58	−42	−18	0	18	22	48
$F(31)$	25	16	−8	−34	−36	−34	−30	−27	−16		
$F(30)$	48	41	24	−29	−23	−27	−28	−29	−18		
$F(42)$	41	36	38								
$F(41)$	35	36	28								
$p_\beta''(0)$ (10^{-3} Å^{-2})	−9.30	−9.23	−9.44	−8.15	−9.02	−9.85	−10.78	−11.04	−10.97	−11.12	−12.27
Γ	64	64	64	16	16	16	16	8	16	4	4
γ	2	2	2	1	2	2	7	5	12	4	4
$\langle\Delta\rho)^4\rangle$	1.544	1.530	1.479	1.469	1.807	1.894	2.487	2.701	3.028	3.422	4.057
type II, case B											
$c_{v,par}$	0.48	0.50	0.54	0.63	0.68	0.71	0.75	0.76	0.77	0.79	0.82
R_{pol} (Å)	26.4	25.4	22.5	17.5	14.3	13.0	11.4	10.9	10.5	9.7	9.0
C_{ch} (Å^2)	46.0	44.7	43.0	38.4	36.7	36.1	33.7	32.4	32.2	30.1	28.1
d (Å)	13.8	14.0	13.8	13.8	13.9	13.3	13.4	13.5	13.5	13.8	14.0

[a] c is the (weight) concentration, a is the parameter of the 2D hexagonal cell, and $F(hk)$ are the structure factors [normalized to $\sum_h\sum_k F^2(kh) = 1000$] with the signs as discussed under Results, section b. The parameters $c_{v,par}$ (volume fraction of the apolar moiety), R_{pol} (radius of the polar cylinder), and S_{ch} (area per chain at the polar/apolar interface) refer to a structure of type II, with the partition of the polar and the apolar moieties of case B (see Results, section a). d ($=0.577a - R_{pol}$) is the maximum distance from any point in the hydrocarbon region to the interface. The columns marked interpolated correspond to virtual samples of phase H at the concentration of the two samples of phase Q_{I5}; the parameters a and $F(hk)$ are interpolated from the corresponding experimental parameters.

segregate at the polar/apolar interface.

(*1*) *Phasing the Reflections.* Phase H is centrosymmetric: the phase angles reduce to signs. A plain argument of physical continuity suggests that if the intensities measured at different concentrations are properly scaled together, then the structure factor of any reflection is a continuous function of c, vanishing at the point c where the sign changes. Reference to more elaborate models is required to correlate the signs of different reflections. We assume here [see Gulik et al. (1985)] that at all concentrations the structure of the rods is related by a similarity. In mathematical terms, this assumption is equivalent to generating a 2D hexagonal packing of circular cylinders of unit radius in a dimensionless space $\mathbf{t} = \mathbf{r}/R_{pol}$; the unit cell parameter is $a^* = a/R_{pol}$, its area $A^* = a^2\sqrt{3}/(2R_{pol}^2) = \pi/c_{v,pol}$. The electron density distribution is $\delta\rho(\mathbf{t})$ inside the cylinder and 0 outside [note that, by definition, $\Delta\rho(\mathbf{t}) + \langle\rho\rangle = \delta\rho(\mathbf{t}) + \rho_{par}$]; the structure factor is $K_cF(\mathbf{s}R_{pol})_{s\neq 0}$, where K_c is a concentration-dependent scaling factor. The application of a well-known theorem yields

$$(1/A^*)\sum_{h\neq 0}(K_cF_h)^2 = \int_{A^*}[\delta\rho(\mathbf{t}) - \langle\delta\rho(\mathbf{t})\rangle]^2 = A^*[\langle(\delta\rho)^2\rangle_{pol}c_{v,pol} - (c_{v,pol}\langle\delta\rho\rangle_{pol})^2] \quad (11)$$

where $\langle\delta\rho\rangle_{pol}$ is the average of $\delta\rho$ over the volume of the polar rods. The function $\delta\rho(\mathbf{t})$ can be normalized by setting, at all c, $\langle\delta\rho\rangle_{pol} = 1$; for the sake of simplicity, we further assume that the electron density is approximately constant inside the polar rods:

$$\langle(\delta\rho)^2\rangle_{pol} \approx (\langle\delta\rho\rangle_{pol})^2 \approx 1 \quad (12)$$

Under these conditions the scaling factor takes the form

$$K_c^2 = (\pi^2c_{v,par})(c_{v,pol}\textstyle\sum_{h\neq 0}F_h^2)^{-1} \quad (13)$$

The experimental values of the structure factors, with their estimated signs, are plotted in Figure 3, in the form $(sR_{pol})^2K_cF(hk)$ vs (sR_{pol}); also drawn is the curve corresponding to the model, namely, the structure factor of a uniform circular cylinder of unit density and unit radius:

$$(sR_{pol})\ J_1(2\pi sR_{pol}) \text{ vs } (sR_{pol}) \quad (14)$$

Although the departure of some of the points from the curve

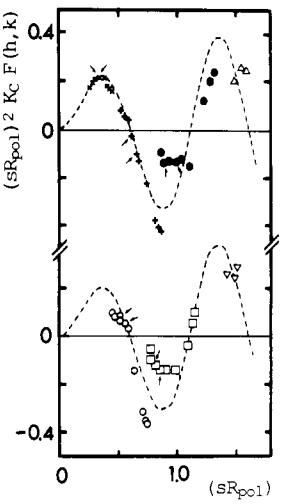

FIGURE 3: Plot of the structure factors of phase H in the form $[(sR_{pol})^2K_cF(hk)]$ vs (sR_{pol}). The structure is supposed to be of type II, case B (see Results, section c). The dotted curve represents the structure factor of a uniform cylinder (eq 10). The upper and lower curves are identical; they are presented twice in order to avoid a confusing overlap of too many symbols. The values of $F(hk)$ are reported in Table III. (hk): ×, (10); +, (20); ●, (30); △, (41); ○, (21); □, (31); ▽, (42). The arrows point at the interpolated points (see Results, section d).

betrays the limited validity of the model, the signs can all be determined unambiguously, with the possible exception of a few of the weakest reflections.

Note that the method above is equivalent to a well-established procedure in the study of partially known structures, namely, to impose the *calculated* phases corresponding to the known part of the structure—in this case the uniform circular cylinders—to the *observed* moduli of the reflections.

(*2*) *Description of the Structure.* The electron density maps (see Figure 4) deserve a few comments, if only because of the rarity of such 2D maps in lipid literature. The isodensity lines are strikingly circular over most of the cell; the absence of conspicuous 6-fold distortions arising from the symmetry of the lattice indicates that a description of phase H in terms of circularly symmetric rods is consistent with physical reality. At the highest lipid concentrations the electron density of the

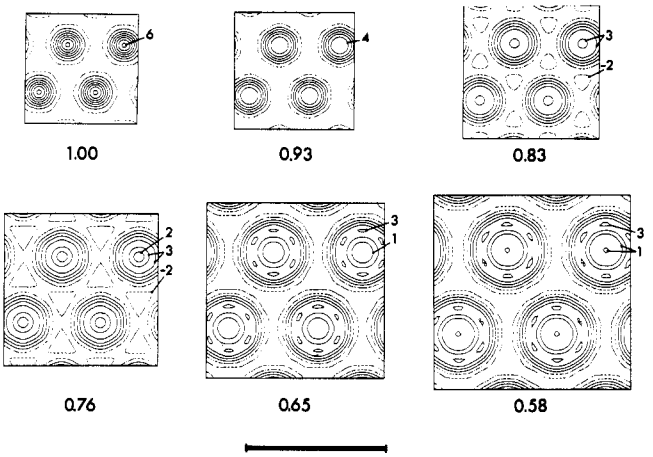

FIGURE 4: A few maps of $\Delta\rho(\mathbf{r})$ for phase H identified by the concentration c. The structure parameters are reported in Table III. The maps are all scaled so that the condition $\langle(\Delta\rho)^2\rangle = 1$ is fulfilled. The equidensity lines are drawn at the levels −1, −0.5, 0, 0.5, 1, ...; the negative levels are dotted. Note that the nonnegative lines—corresponding to the polar regions—are almost perfectly circular and that the negative (hydrocarbon) regions are very flat; note also that the radius of the 0 contour line (close to the polar/apolar interface) is very close to R_{pol} (reported in Table III). The bar represents 100 Å.

polar rods takes the form of a monotonic peak; as the amount of water increases, the peak flattens out and eventually displays a minimum, in keeping with the low electron density of water. In contrast, all the maps are flat over the hydrocarbon region. Besides, the diameters of the polar rods as determined by chemical considerations (see Table III) are at all concentrations in excellent agreement with the diameter of the zero level isodensity lines.

(d) Cubic Phase. An optically isotropic and highly viscous cubic phase is easily identified in the phase diagram, straddled by the hexagonal phase (Figure 1).

The reflections systematically absent are $h + k$, $k + l$, and $h + l \neq 2n$ for the general reflections (hkl) and $k + l \neq 4n$ for the zone $(0kl)$ (with circular permutations). These absences suggest that the lattice type is face-centered and that the cubic aspect is no. 15. Two space groups are compatible with that cubic aspect: Q^{203} and Q^{227} ($Fd3$ and $Fd3m$, respectively). The two space groups are centrosymmetric and belong to different Laue classes: Q^{203} to $m3$ and Q^{227} to $m3m$. As a consequence, the intensities of any pair of noncylically related reflections are different for Q^{203} and equal for Q^{227}. Since Q^{227} corresponds to special positions of Q^{203}, one way out of the dilemma would be to adopt the more general space group and to treat each pair of reflection $\{F(hkl), F(khl)\}_{h\neq k\neq l}$ as a noncentric reflection (namely, to share the observed intensity between the two reflections). We have met the same problem in the study of another cubic phase (Q_4 of monoolein; Mariani et al., 1988); taking into account the conclusions of that analysis, and also the fact that only two of the observed reflections—(531) and (620), both very weak or absent (see Table IV)—belong to that class, we adopt here the space group with highest symmetry, confident that the final result will be barely sensitive to that choice. We henceforth name the phase Q^{227}.

(l) Phasing the Structure Factors. In the case of *P. fluorescens* lipids, the cubic phase was observed over a fairly narrow concentration range, bordered by phase H both at high and at low concentration (Figure 1); the circumstances are thus particularly favorable to screening the φ-sets of the cubic phase by using the hexagonal phase as a reference. In the previous applications of the technique we were cautious to compare phases whose chemical composition was almost identical and to let both the cutoff s_{max} and the curvature $p_\beta''(0)$ take the same value in the two phases being compared (Luzzati et al., 1988; Mariani et al., 1988). Since the data analyzed in this work are more extensive than any of those previously available, we though it worthwhile to look more carefully into the influence of the various parameters on the phasing procedure. For that purpose we computed the values of $p_\beta''(0)$ and $\langle(\Delta\rho)^4\rangle$ as a function of c and for various choices of β^2 using the structure factors of Tables III and IV; in the case of the cubic phase, $\langle(\Delta\rho)^4\rangle$ corresponds to the φ-set of rank 1 in Table VII. Different plots of these parameters are presented in Figure 5.

Several points emerge from the figure. First, $p_\beta''(0)$ is bounded in the range $[(2\pi s_{max})^2/3] \leq [-p_\beta''(0)] \leq [(2\pi s_{min})^2/3]$ (s_{min} and s_{max} correspond to the first and to the last reflection of that particular experiment); therefore, if $-p_\beta''(0)$ is too small (6, 8, and 10×10^{-3} Å^{-2} in rows 2–5), then some of the points drop out of the graph. Second, the graph $\langle(\Delta\rho)^4\rangle$ vs c obtained with the raw nonapodized data is regular and follows quite closely the curve corresponding to an ideal two-step map; this is also true for the apodized data, at least when the apodization is not too drastic [$-p_\beta''(0) \geq 8 \times 10^{-3}$ Å^{-2}] and the data are not truncated (compare rows 3 and 5). Third, truncating the data has the awkward effect of introducing a discontinuity in the curve $\langle(\Delta\rho)^4\rangle$ vs c at the point c where the cutoff coincides with the position of one reflection; this effect is dramatic in the regions bordering the cubic phase, which play a critical role in the phasing procedure (see Figure 6).

Therefore, we decided to make use of all the observed reflections, without truncation, in the comparison of hexagonal and cubic phases, and to introduce a mild apodization, adjusting the parameter $p_\beta''(0)$ to a value intermediate between

Table IV: Parameters of the Cubic Phase[a]

c	0.86	0.89	0.90	0.91
a (Å)	146.2	133.9	133.0	129.6
$F(111)$	20			20
$F(220)$	79			80
$F(311)$	107			109
$F(222)$	270			273
$F(400)$	55			50
$F(331)$	21			20
$F(422)$	12			11
$F(511)$	17			14
$F(333)$	17			14
$F(440)$	24			19
$F(531)$	9			
$F(442)$	10			
$F(620)$	14			10
$F(533)$	12			
$F(622)$	12			
$p_\beta''(0)$ (10^{-3} Å^{-2})	−7.61			−9.24
Γ	8192			512
γ	1			1
$\langle(\Delta\rho)^4\rangle$	2.252			2.736
type II, case B				
$c_{v,par}$	0.71	0.73	0.74	0.75
L_{rod} (Å)	63.3	58.0	57.6	56.1
R_{rod} (Å)	14.1	11.9	11.7	10.9
R_{sph} (Å)	18.4	16.4	16.2	15.6
S_{ch} (Å^2)	34.7	34.4	34.1	33.7

[a] Notation as in Table III. Four samples were studied; the intensities of only two were measured. The raw normalized structure factors are reported, with the signs corresponding to the maps in Figure 9. The partition of the intensity of the Debye–Scherrer ring, $h^2 + k^2 + l^2 = 27$, between the reflections (511) and (333) is discussed under Results, section d. The radii of the rods (R_{rod}) and of the spherical micelles (R_{sph}) are consistent with the total polar volume and with the area per chain being the same in the two types of structure elements (see text).

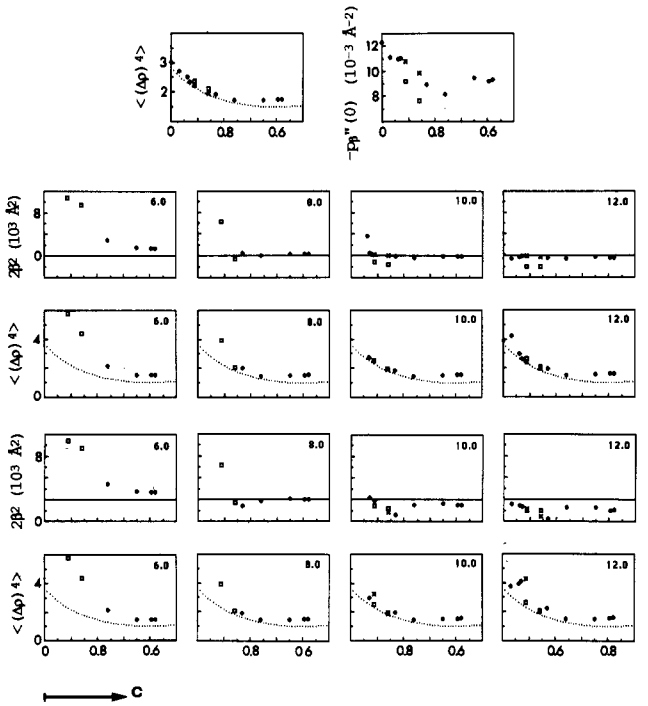

FIGURE 5: (Row 1) Plots of $\langle(\Delta\rho)^4\rangle$ vs c and $p_\beta''(0)$ vs c for the raw, nonapodized data reported in Tables III and IV. (Rows 2 and 3) Plots of $2\beta^2$ vs c and $\langle(\Delta\rho)^4\rangle$ vs c for apodized, nontruncated data with preimposed values of $p_\beta''(0)$ (labeled in each frame, in units -10^{-3} Å^{-2}). (Rows 4 and 5) As in rows 3 and 4 but with the data of phase H truncated at the same s_{max} as those of phase Q_{15}. (□) phase Q_{15}; (●) experimental phase H; (×) interpolated phase H. The dotted lines represent the calculated function $\langle(\Delta\rho)^4\rangle = \{1 + c_1[(c_2/c_1)^4 - 1]\}\{1 + c_1[(c_2/c_1)^2 - 1]\}^{-2}$, corresponding to a two-step density distribution whose volume fractions are $c_1 = c_{v,pol}$ and $c_2 = c_{v,par}$.

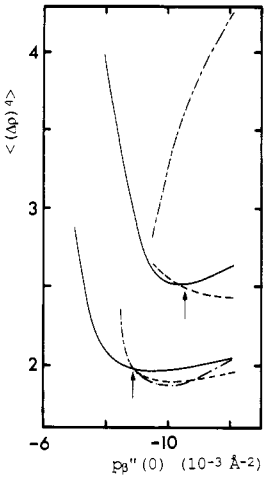

FIGURE 6: Function $\langle(\Delta\rho)^4\rangle$ vs $p_\beta''(0)$ calculated for phase Q_{15} (solid lines) and for phase H, either with all the observed reflections (dotted lines) or with data truncated at the same s_{max} as the data of phase Q_{15} (hatched lines). The upper curves correspond to $c = 0.91$ and the lower ones to 0.86. The amplitudes of the structure factors are reported in Tables III (columns marked interpolated) and IV; the signs correspond to the φ-sets of rank 2 and 7 for phase H (Table VI) and of rank 4 and 12 for phase Q_{15} (Table VII). The arrows mark the points adopted for the comparison. Note that the curves are fairly flat in the vicinity of the arrows with the remarkable exception of the curve relevant to phase H, truncated data, $c = 0.91$.

those relevant to the raw data of the two phases. We carried out the comparison on two pairs of samples: those of the cubic phase correspond to the experiments performed at $c = 0.86$ and 0.91; those of the hexagonal phase correspond to virtual experiments whose cell parameter and structure factors are determined by interpolation of the c-dependent experimental

Table V: Some Parameters of Samples Involved in Phasing the Reflections of Q_{15}[a]

	c	0.86		0.91	
	phase	H	Q_{15}	H	Q^{15}
raw data	$2\beta^2$ (Å^2)	0	0	0	0
raw data	$p_\beta''(0)$ (10^{-3} Å^{-2})	−9.85	−7.61	−10.78	−9.24
raw data	s_{max} (10^{-2} Å^{-1})	7.61	4.54	8.17	4.88
apodized	$2\beta^2$ (Å^2)	373	−1094	64	−1472
apodized	$p_\beta''(0)$ (10^{-3} Å^{-2})	−8.88	−8.88	−10.5	−10.5
	$\langle(\Delta\rho)^4\rangle$	1.980	1.979	2.496	2.501

[a] The concentrations of the two samples of phase Q_{15} used in the analysis are 0.86 and 0.91; the experimental parameters a and $F(hk)$ of phase H were interpolated at those concentrations (see Table III). Rows 3 and 4 report the values of $2\beta^2$ and of $p_\beta''(0)$ relevant to the raw data; the values corresponding to the apodized data are given in rows 6 and 7. Also reported are the position s_{max} of the cutoff and the value of $\langle(\Delta\rho)^4\rangle$.

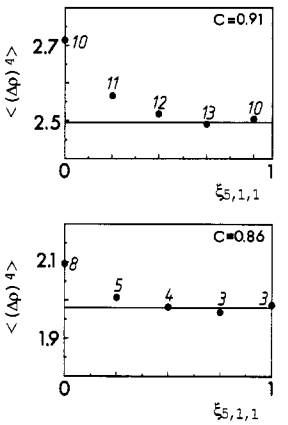

FIGURE 7: Function $\langle(\Delta\rho)^4\rangle$ vs ζ_{511} for the two cubic samples. The parameter ζ_{511} [$=m_{511}F_{511}^2/(m_{511}F_{511}^2 + m_{333}F_{333}^2)$, where m_{hkl} is the multiplicity factor] specifies the distribution of the intensity of the Debye–Scherrer ring, $h^2 + k^2 + l^2 = 27$, between the reflections (511) and (333). For each value of ζ_{511}, all the φ-sets were generated by using the raw, nonapodized structure factors; the minimum value of $\langle(\Delta\rho)^4\rangle$ is reported. Each φ-set is labeled by reference to Table VII. The horizontal line indicates the value of $\langle(\Delta\rho)^4\rangle$ of the corresponding phase H, interpolated and apodized (see Table V).

values. The cell parameters and the raw structure factors are reported in Tables III and IV; the values of the parameter $2\beta^2$ used in the apodization are given in Table V.

Each Debye–Scherrer ring of Table IV corresponds to one single reflection, with the exception of the pair {(511), (333)}. Consequently, one variable, ζ_{511}, was added to the φ-set: this variable—$\zeta_{511} = m_{511}F_{511}^2/(m_{511}F_{511}^2 + m_{333}F_{333}^2)$, where m_{hkl} is the multiplicity factor (Mariani et al., 1988)—specifies the distribution of the intensity of the ring, $h^2 + k^2 + l^2 = 27$, between the two reflections. The ζ_{511} dependence of $\langle(\Delta\rho)^4\rangle$ is shown in Figure 7: we decided to adopt $\zeta_{511} = 0.5$, with the understanding that the final result is barely sensitive to that choice.

We report in Table VI a list of φ-sets with the corresponding value of $\langle(\Delta\rho)^4\rangle$. The screening process, which involves the comparison of phases H and Q^{227}, will be centered on the apodized data, with special emphasis on the experiments at $c = 0.86$ which are more complete (see Table IV); the maps, on the contrary, will all be computed by using the raw data.

With the apodized data, the φ-sets whose $\langle(\Delta\rho)^4\rangle$ best agrees with the corresponding hexagonal phase are those of rank 4 at $c = 0.86$ and rank 9 at $c = 0.91$ (arrows in Table VII). When the analysis is performed with the raw data, those φ-sets move to ranks 1 and 16, respectively; at the two concentrations, moreover, the same φ-set is found at rank 1 (underlined in Table VII). Therefore, this φ-set seems to be

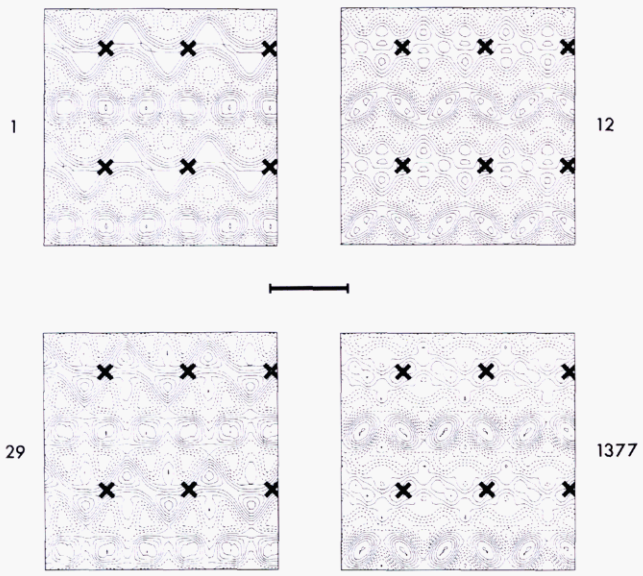

FIGURE 8: Experiment $c = 0.86$ for phase Q_{15} (space group $Fd3m$) (see Table IV). Shown are sections (110) through the origin of the maps relevant to the φ-sets of highest rank (Table VII, column $2\beta^2 = 0$) of each of the four families corresponding to fixed signs of the reflections (220) and (400) (see text). Each map is labeled by the rank of the φ-set. The signs of the reflections (220) and (400) are $-+$ for rank 1, $+-$ for rank 12, $--$ for rank 29, and $++$ for rank 1377. Note that the map of rank 1 is the most regular. In this figure, as in Figure 9, a cross marks the origin of the cell, the bar represents 100 Å, the density levels are all equally spaced with an increment of 0.5, and the negative levels are dotted.

the most likely candidate; more cautiously, we conclude that the "best" φ-set lies somewhere at the top of Table VII. The final selection involves the inspection of the maps in a search for consistency with the chemical properties of the sample (see below). On this ground, and after inspecting some 30-odd maps at the top of the table, we eventually chose the φ-set underlined in Table VII, the same and of rank 1 at the two concentrations.

Some aspects of the screening process should be discussed.

The discrimination between a "satisfactory" and an "unsatisfactory" map can be illustrated as follows. According to the maps, the φ-sets can be sorted out into four families, each corresponding to a particular choice of the phases of the strongest reflections [(220) and (400), since the signs of (311) and (222) are fixed; see Materials and Methods, section e]; within each family the maps are similar to each other. Using the raw data at $c = 0.86$, we computed for each family the map whose $\langle(\Delta\rho)^4\rangle$ is minimum: the section (110) of those maps is reported in Figure 8. Clearly the map of rank 1 is smoother and more regular than any of the others, and its features are in better agreement with the chemical properties of the system (see Description of the Structure below).

The effects of apodization are best summarized in Figure 6, in which the function $\langle(\Delta\rho)^4\rangle$ vs $p_\beta''(0)$ is plotted for the two phases. The odd consequences of truncating the data are conspicuous in the case of phase H, at $c = 0.91$. Regarding the nontruncated data, it is rewarding to note that, in the vicinity of the point $p_\beta''(0)$ adopted in the analysis, the curves are all reasonably flat: in other words, the choice of $p_\beta''(0)$ does not seem to play a critical role.

(*2*) *Description of the Structure.* A few sections of the map are presented in Figure 9. The positive regions delineate an infinite 3D network of rods (green in Figure 9), tetrahedrally

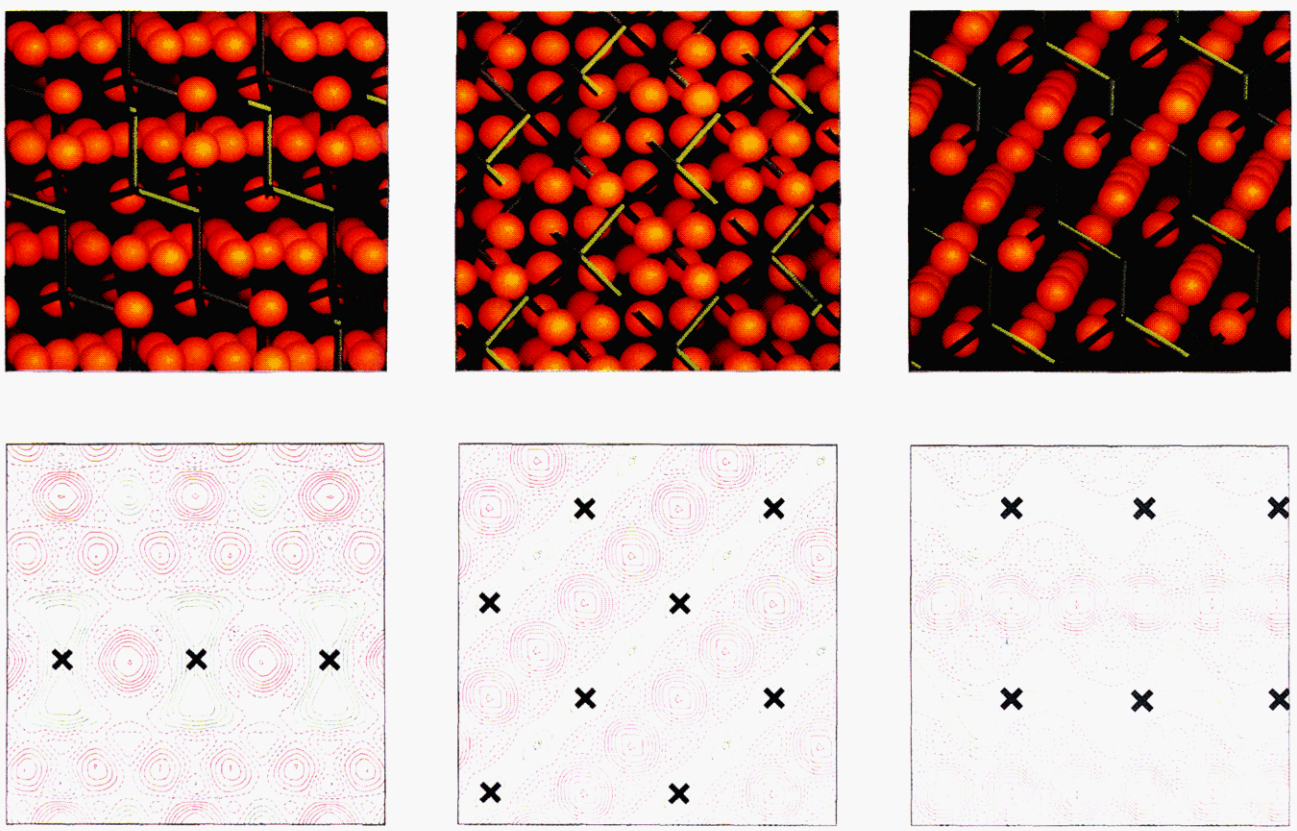

FIGURE 9: Same experiment as in Figure 8 with φ-set of rank 1. (Lower frames) Three planar sections through the origin of the map of rank 1: left, (112); middle, (001); right, (110). The positive levels are red inside the globular micelles and green in the rods. Note that rods and micelles are all disjointed: no positive equidensity line connects micelles to micelles, micelles to rods, or rods to rods. (Upper frames) Perspective views of the structure slightly off the normal to the planes of the sections. The micelles are represented by orange spheres and the axes of the rods by green bars. Note the 3D network of rods joined tetrahedrally four by four and the system of disjointed micelles.

Table VI: φ-Sets of Phase H[a]

c	0.86		0.91	
$2\beta^2$	373 (Å^2)		64	
$p''_\beta(0)$	-8.9 (10^{-3} Å^{-2})		-10.5	
γ	φ-set	$\langle(\Delta\rho)^4\rangle$	γ	φ-set	$\langle(\Delta\rho)^4\rangle$
1	+---+	1.961	1	+---+	1.857
2	+----	1.980	2	+----	1.945
3	+--+-	2.153	3	+-+-+	2.062
4	+--++	2.175	4	+-+--	2.131
5	++---	2.298	5	+--+-	2.182
6	++--+	2.312	6	+--++	2.215
7	+-+--	2.393	7	++---	2.496
8	+-+-+	2.396	8	+-++-	2.517
9	++-+-	2.565	9	++--+	2.539
10	++-++	2.634	10	+-+++	2.575
11	+-++-	2.744	11	+++--	2.790
12	+-+++	2.791	12	+++-+	2.881
13	++++-	2.824	13	++-+-	2.988
14	+++-+	2.871	14	++-++	3.248
15	++++-	3.288	15	++++-	3.463
16	+++++	3.396	16	+++++	3.785

[a] The φ-sets are ranked in the order of increasing $\langle(\Delta\rho)^4\rangle$. The two sets of data correspond to virtual experiments, interpolated at the concentration of the the two cubic samples and apodized (Table V). The signs refer to the structure factors, sorted in the order of increasing s (Table III). The selected φ-sets are underlined.

joined 4 by 4, and a family of identical quasi-spherical globules (red in Figure 9); the two types of structure elements are disjointed, in the sense that each of the globules is separated from the other globules and from the rods by regions of negative density. The axes of the rods, organized according to a diamond lattice, occupy position e, of symmetry $3m$; the globules, of symmetry $3m$, are centered at positions c (*International Tables*, 1952). A schematic representation of the structure in terms of rods and spheres is shown in Figure 9.

The structure lends itself to chemical verification. By analogy with phase H (see Results, section c, and Figure 2), we presume that the structure is of type II: the rods and the globules are filled by the polar moiety, their surface is lined by the polar headgroups, and the interstices are occupied by the hydrocarbon chains. We also assume that the headgroups of the fatty acids are located at the polar/apolar interface (case B; see Results, section a). The map is smooth and regular inside the rods and the globules; the density, moreover, takes similar values in the two structure elements (and also in the maps of phase H; see Figure 4). By analogy with the calculations given under Results, section c, and taking into account the volume and the area of the network of tetrahedrally joined and bevel-shaped rods (Gulik et al., 1985), we calculate the polar volume and the interfacial area per face-centered unit cell [each cell contains 16 rods of length $L_{rod} = (\sqrt{3}/4)a$ and radius R_{rod} and 16 globules, supposed to be spheres of radius R_{sph}]:

$$V_{pol} = a^3 c_{v,pol} = 16(4\pi/3)R_{sph}^3 + 16\pi R_{rod}^2 L_{rod}(1 - 0.780R_{rod}/L_{rod}) \quad (15)$$

$$S = 16(4\pi)R_{sph}^2 + 32\pi R_{rod}L_{rod}(1 - 1.068R_{rod}/L_{rod}) \quad (16)$$

Assuming, moreover, that the chemical composition is the same in the rods and the globules, we determine the radius of the two structure elements under the constraint that S_{ch} is equal in the two. The results (reported in Table IV and Figure 2) are in remarkable agreement with those of phase H; the radii, moreover, closely agree with the dimensions of the volumes enclosed by the isodensity surface $\Delta\rho(\mathbf{r}) = 0$. Besides, no point within the hydrocarbon matrix is further away from the polar/apolar interface than the fully extended length of the average hydrocarbon chain [see Gulik et al. (1985)].

Discussion and Conclusions

One of the aims of this work was to take advantage of the unusual circumstance of a cubic phase straddled by a hexagonal phase to test the validity and to improve the implementation of the novel approach to crystallographic structure analyses at very low resolution. Phasing the reflections of the hexagonal phase was not a trivial problem: we resorted to a procedure that is heavily dependent upon the presence of a high-density cylindrical core, whose diameter can be estimated by using chemical arguments. Regarding the strategy of screening the φ-sets, the results of this work verify and reinforce the assumption that in phases of different structure—but with the same chemical composition—$\langle(\Delta\rho)^4\rangle$ is invariant, provided that the maps are normalized both in value ($\langle(\Delta\rho)^4\rangle = 1$) and in shape [$p_\beta''(0)$ is equal in the two phases]. An analysis of the influence of various parameters on $\langle(\Delta\rho)^4\rangle$ shows that (i) $\langle(\Delta\rho)^4\rangle$ is strongly dependent on $p_\beta''(0)$; (ii) in comparing samples of different phases, the crystallographic data should be brought to the same concentration, possibly by extrapolation; (iii) the data should be truncated artificially in reciprocal space; and (iv) the value of $p_\beta''(0)$ should be adjusted by apodization in reciprocal space. When all these precautions were taken, $\langle(\Delta\rho)^4\rangle$ took remarkably close values in the two phases, reinforcing the conclusion that this parameter provides an excellent test to screen the φ-sets. Besides, the comparison of the empirical curves $\langle(\Delta\rho)^4\rangle$ vs c with the curve relevant to an ideal two-step distribution (see Figure 5) indicates that such simple distribution yields a useful first-order approximation. It must also be noted that, for the cubic but not for the hexagonal phase, the "best" maps are also those whose $\langle(\Delta\rho)^4\rangle$ is minimum (namely, the smoothest, whose entropy is maximal; Mariani et al., 1988). All these observations are of great interest in view of future applications of this novel phasing technique to low-resolution crystallographic problems of more general interest.

The purpose of the novel pattern recognition approach—the point is worth stressing—is to spin a thread to help one find his way out of the labyrinth of phase space, rather than to set a rigid track leading infallibly to the structure. More modestly the technique, when properly implemented, has the effect of cutting down (from 8192 to approximately 30 in the example of Table VII) the number of φ-sets worth taking into account: independent criteria must be used to find out which of the issues is satisfactory. As a rule, moreover, the question of uniqueness has no answer in crystallographic analyses: structures must be justified a posteriori by crystallographic, chemical, and other (EM, NMR, etc.) arguments. In the case of the hydrated lipid phases the "resolution" of the data is generally much too low, and the structures are too complex, to justify a schematic representation of the structure in terms of elements of simple shape, like atoms in high-resolution structure determinations [the case of the anhydrous Sr soaps is exceptional; see Results, section e, and also Mariani et al. (1988)]; as a consequence the comparison of the observed and the calculated structure factors is of little help. The most useful tests hinge upon chemical criteria, especially when these criteria were not involved in the crystallographic analysis. In protein crystallography, for example, the phases of the reflections are determined by straightforward techniques (multiple isomorphous replacements, anomalous scattering) that do not involve chemical information; eventually, the phases are verified by the correlations of the maps with known chemical features (for example, tracing of continuous polypeptide chains). In the case of the cubic phase discussed in

Table VII: φ-Sets of Phase Q_{15}[a]

c		0.86				0.91			
$2\beta^2$	(Å^2)	-1094		0		-1472		0	
$p''_\beta(0)$	(10^{-3} Å^{-2})	-8.9		-7.61		-10.5		-9.24	
φ-set		γ	$\langle(\Delta\rho)^4\rangle$	γ	$\langle(\Delta\rho)^4\rangle$	φ-set	γ	$\langle(\Delta\rho)^4\rangle$	γ	$\langle(\Delta\rho)^4\rangle$
---+++----+++-+-		1	1.936	2	2.270	-+-+-++---+00-00	1	2.279	3	2.784
---+++---++-+-+		2	1.937	5	2.333	---+++----00+00	2	2.305	2	2.742
---+++----+-++-		3	1.959	3	2.272	++-+-+---+00-00	3	2.370	11	2.923
---+++----++-+-		4	1.979 ←	1	2.252	+--+++----00+00	4	2.415	14	2.941
+--+++----+-++-		5	1.992	7	2.380	---+++---00-00	5	2.425	4	2.852
+--+++---+-+-+-		6	2.012	16	2.451	-+-+-+----+00-00	6	2.436	7	2.900
---+++-+---+-+-		7	2.017	6	2.357	+--++++---00-00	7	2.480	23	3.015
+--+++-----+++-		8	2.026	10	2.415	+++-+-+---+00-00	8	2.482	21	2.988
-+-+-++--+++-+-		9	2.044	12	2.417	---+-+----+00-00	9	2.501 ←	16	2.948
+--+++----+-+-+-		10	2.049	8	2.389	-+-+-++-++00-00	10	2.502	19	2.967
+--+++---+---+-		11	2.055	14	2.442	+---+----+00-00	11	2.505	18	2.950
++-+-++--+--+-+		12	2.072	17	2.459	---++++---00-00	12	2.518	1	2.736
---+++--+-++++-		13	2.085	13	2.440	---+++--+-+00+00	13	2.526	10	2.917
++-+-++---+++-+-		14	2.085	24	2.489	+--+++----00-00	14	2.546	12	2.923
---++++-+-++-+-		15	2.090	31	2.508	++-+-++-++00-00	15	2.569	30	3.065
---+++----+--+-+		16	2.105	4	2.292	-+-+-+---+00+00	16	2.594	13	2.934
-+-+-++--+-+--+-		17	2.107	15	2.443	---++++-+-00-00	17	2.613	26	3.034
+++-+-++-+++-+-		18	2.130	73	2.599	---+++---00+00	18	2.618	17	2.949
+--+-+---+-+--+-		19	2.130	29	2.501	+---+++--+-00+00	19	2.631	45	3.124
---+++------++-+-		20	2.134	18	2.459	++-+-+----+00+00	20	2.683	27	3.047
+---+-+---+++-+-		21	2.141	37	2.529	+--++++-+-00-00	21	2.695	68	3.209
+--+++----+---+-		22	2.141	9	2.400	+--+++---00+00	22	2.703	42	3.108
+--+++--+-++++-		23	2.146	57	2.577	---+-+--++00-00	23	2.718	48	3.149
-+-+-++-+++-+-		24	2.151	63	2.587	------+-+-00-00	24	2.733	8	2.900
---+-+---+++-+-		25	2.154	51	2.569	+--+-+--++00-00	25	2.736	47	3.145
---+++-----+++-		26	2.155	19	2.464	-+-+-+++-+00-00	26	2.739	24	3.017
+--++++-+++-+-		27	2.159	92	2.627	+---+++--+00-00	27	2.749	72	3.220
---+++--+-++-+-		28	2.164	11	2.416	-+-+-+--++00-00	28	2.780	46	3.133
+--+++-----+++-		29	2.167	40	2.534	---+++-+--00+00	29	2.784	39	3.106
--+-+-+---+---+-		30	2.168	30	2.507	+--+-+----00+00	30	2.788	15	2.944
-+-+-+++-+++-+-		31	2.169	59	2.585	+--+++--+-00-00	31	2.792	40	3.107
+++-+-+---++--+-		32	2.170	39	2.534	+--+-+----+00+00	32	2.800	33	3.067
---+-----++----		512	2.626	518	2.914	++-+-++---00-00	48	2.933	32	3.067
---+-++---+----		1024	2.836	917	3.051	+++-+--++00+00	64	3.052	76	3.233
---+-++--+-+---		1536	3.014	1494	3.213	+--+++-+--00-00	96	3.166	99	3.324
++-+-+---+++++-		2048	3.171	1250	3.144	+--+-+-+--00+00	128	3.307	90	3.303
+--+-+--+-----+		2560	3.350	1855	3.300	-+-+-+-+--00+00	160	3.443	121	3.382
---+-+--+-----++		3072	3.535	1570	3.233	++-++-+---00-00	192	3.556	397	4.331
+--+----++++--		3584	3.700	4595	3.934	-+-+------00+00	224	3.642	169	3.541
-+-+------++++		4096	3.867	3223	3.609	---+---++-00+00	256	3.734	227	3.695
++-+-----++-+--		4608	4.050	4982	4.038	++-+--+++-00-00	288	3.858	315	3.953
+--+-+++--+---+		5120	4.248	4304	3.862	-+-+---++-00+00	320	4.014	310	3.924
-+-+-+++---+--+		5632	4.453	3597	3.693	-+-+----++-00-00	352	4.234	304	3.912
+--+-----+++-++		6144	4.694	6571	4.570	---++-+---+00+00	384	4.427	331	4.011
++-+-+--+-+----		6656	4.996	7423	5.079	---+++---++00-00	416	4.641	360	4.127
+--+-+++----+-+		7168	5.418	6426	4.510	+--+++++-+00+00	448	4.937	377	4.200
+--++-+++++++-		7680	6.110	7873	5.614	-+-++-++-+00+00	480	5.647	473	4.899
++-++-++++--++-		8192	10.380	8190	7.568	+--+++++00+00	512	7.033	508	5.533

[a] See legend of Table VI. The signs refer to the reflections given in Table IV. All the φ-sets are generated and sorted out in the order of increasing $\langle(\Delta\rho)^4\rangle$. The 32 top φ-sets are reported and also a few examples of the following ones. Columns 2, 3, 7, and 8 correspond to the apodized structure factors (Table V) and columns 4, 5, 9, and 10 to the raw data. In all cases $\zeta_{5,1,1}$ was taken equal to 0.5 (see Figure 6). The arrows point at the φ-sets whose $\langle(\Delta\rho)^4\rangle$ are closest to those of the corresponding hexagonal phase (see Table VI). The φ-set chosen as "best", the same at the two concentrations, is underlined.

this work the maps were obtained by using purely mathematical procedures; the maps themselves revealed the presence of the 3D network of rods and of the quasi-spherical micelles. Therefore, the structure is supported by the whole of the crystallographic data—dimension and symmetry of the unit cell, intensity of the reflections—and by its chemical properties; more precisely (see Results, section d), the map is smooth and regular, the volume fractions of the positive and the negative regions are close to $c_{v,pol}$ and to $c_{v,par}$, and the diameter and the surface area of rods and globules, as well as the dimensions of the low-density regions, agree with the molecular dimensions.

We have surmised [reviewed by Mariani et al. (1988)] that, as a consequence of the short-range disorder, the symmetry of both the space group and the structure elements is likely to be the highest compatible with the data: it is rewarding to note that the high-density regions of the maps are indeed *clustered* around 3-fold axes and points of symmetry $3m$, thus justifying the description of the structure in terms of rods and globules.

The structure of phase Q^{227}, like that of four of the other five cubic phases known so far, is bicontinuous in the sense (Luzzati & Spegt, 1967) that both the apolar and part of the polar volumes are continuous throughout the 3D space. The structure subdivides space into one polar—the 3D network of rods—and one apolar continuum; the apolar medium, moreover, encloses a system of disjointed reversed micelles. We have called this type of structure (to which phase Q^{212} also belongs) the *bicontinuous monolayer*, by contrast with the *bicontinuous bilayer* type (phases Q^{230}, Q^{224}, and Q^{229}) in which three disjointed continuums are present: two—of the same polarity—are separated from each other by a septum of opposite polarity (Mariani et al., 1988). The fact is noteworthy that the topology of the structure of phase Q^{227} requires that some of the interfaces (globule/globule, rod/globule, rod/rod) intersect each other; consequently, the structure (like that of phase Q^{212}) does not belong to the family of the *infinite periodic surfaces without intersections* (IPSI) (Hyde et al., 1984) to which on the contrary belong phases Q^{230}, Q^{224}, and Q^{229} (Mariani et al., 1988).

In an early attempt to rationalize the polymorphism of lipid phases, we surmised that infinite polar lamellae (or infinite

straight rods) may be destabilized whenever the steric requirements of the polar headgroups and of the hydrocarbon chains cannot both be satisfied at once; we speculated that one way to release the constraints is to fragment the lamellae into ribbons or disks (or the cylinders into short rods, linked together in a network). Those operations were expressed in terms of qualitative concepts like "relative bulkiness" and "cumulative strains effects" [reviewed by Luzzati and Tardieu (1974)]. Recently, Charvolin and Sadoc (1988) have put forward a more formal treatment of the problem in terms of lipid layers, frustrations, and disinclinations. According to those authors, one way to release the constraints and to preserve the structural equivalence of the two faces of the bilayer is to fold the lipid lamella in a cubic lattice corresponding to one of the IPSI structures (for lipid phases, Q^{230}, Q^{224}, or Q^{229}, see above). As noted previously (Mariani et al., 1988), phase Q^{227} derives from phase Q^{224} (as phase Q^{212} from phase Q^{230}; Mariani et al., 1988) by removing one of the two 3D networks of water channels and replacing it by a system of disjointed globules. This operation transforms the symmetric bilayer into an asymmetric monolayer (see above). Most likely, this symmetry-breaking process mirrors an uneven segregation of the different lipid species between the two types of structure elements. *P. fluorescens* lipids, as all the other lipid preparations that so far have been found to yield phase Q^{227}, are indeed chemically heterogeneous: fatty acids, moreover, are a ubiquitous component. It would be interesting to investigate the chemical nature of this puzzling segregation; other techniques, for example, neutron scattering of specifically labeled samples, are required for that purpose.

In biological circles cubic phases—and more generally the whole lot of the nonlamellar lipid phases—were at one time looked down upon as mere crystallographic oddities unworthy of serious consideration. Times have changed: first the hexagonal phases became fashionable [reviewed by Seddon (1989)] and later the cubic phases turned out to be so multifarious and omnipresent that discussing their structure and questioning their significance became popular exercises [reviewed in Mariani et al. (1988); see also Lindblom and Rilfors (1989)]. Regarding more specifically phase Q^{227}, two facts should be stressed. First, the phase has been observed in several commercial cosmetic preparations (Gulik-Kryzywicki, unpublished) presumably designed to meet practical requirements; how, then, is structure related to the properties of practical interest? Second, in an attempt to simulate the physiological digestion of fats, Mariani et al. (1988) studied a mixture of monoolein and oleic acid; they discovered phase Q^{227} in equilibrium with excess water and at acidic pH. An unidentified cubic phase had been previously observed by Patton (1981) in the course of the in vitro enzymatic digestion of triglycerides. The digestion of fats is an unusual enzymatic reaction since both the substrate (triglycerides) and the products (monoglycerides and fatty acids) are insoluble in the reaction medium: one may wonder how the enzyme molecules reach the substrate and the reaction products move away from the substrate. The structure of phase Q^{227} may provide a solution to the problem. The diameter of the rods of the water 3D lipid network is sufficiently large (50 Å in the system monoolein–oleic acid; Mariani et al., 1988) as to leave ample room for the lipase molecules to find their way to the substrate; the reaction products, in turn, may diffuse in the hydrocarbon matrix, along the rods or incorporated in the micelles [see also Luzzati et al. (1987)]. According to this view, the generation of the cubic phase may be visualized as an autocatalytic mechanism whereby the enzymatic reaction builds up a structure that, in turn, promotes the propagation of the reaction.

Two final comments: First, although it is generally assumed that all phases with the same cubic aspect belong to the same space group and have the same structure (Mariani et al., 1988), the possibility is quite open that the rule may have exceptions, especially among the numerous phases with cubic aspect Q_{15} observed in systems of such widely different chemical compositions (see the introduction). Second, structure models consisting of open and/or closed elements lend themselves to tests based upon pulsed gradient NMR experiments.

Acknowledgments

We are grateful to Jean-Claude Dedieu for competent assistance in drawing the figures.

References

Charvolin, J., & Sadoc, J. F. (1988) *J. Phys. Chem. 92*, 5787–5792.
Das, S., & Rand, R. P. (1986) *Biochemistry 25*, 2882–2889.
Folch, J., Lees, M., & Sloane-Stanley, G. H. (1957) *J. Biol. Chem. 226*, 497–509.
Gill, C. O. (1975) *J. Gen. Microbiol. 89*, 293–298.
Gulik, A., Luzzati, V., DeRosa, M., & Gambacorta, A. (1985) *J. Mol. Biol. 182*, 131–149.
Gulik-Krzywicki, T., Rivas, E., & Luzzati, V. (1967) *J. Mol. Biol. 217*, 303–322.
Hyde, S. T., Andersson, S., & Larsson, K. (1984) *Z. Kristallogr. 168*, 213–219.
International Tables for X-ray Crystallography (1952) Kynoch Press, Birmingham, U.K.
Kates, M. (1960) *Biochim. Biophys. Acta 41*, 315–328.
Larsson, K. (1968) *Z. Phys. Chem. (Munich) 56*, 173–198.
Lindblom, G., & Rilfors, L. (1989) *Biochim. Biophys. Acta 988*, 221–256.
Lowry, O. H., Rosenbrough, N. J., Farr, A. L., & Randall, R. J. (1951) *J. Biol. Chem. 193*, 265–275.
Luzzati, V. (1968) *Biological Membranes* (Chapman, D., Ed.) Vol. 1, pp 71–123, Academic Press, London and New York.
Luzzati, V. (1981) *J. Physiol. (Paris) 77*, 1025–1028.
Luzzati, V., & Husson, F. (1962) *J. Cell Biol. 12*, 207–219.
Luzzati, V., & Spegt, P. A. (1967) *Nature (London) 215*, 701–704.
Luzzati, V., & Tardieu, A. (1974) *Annu. Rev. Phys. Chem. 25*, 79–94.
Luzzati, V., Gulik, A., Gulik-Krzywicki, T., & Tardieu, A. (1986) *Lipids and Membranes: Past, Present and Future* (Op den Kamp, J. A. F., Roelofsen, B., & Wirtz, K. W. A., Eds.) pp 137–151, Elsevier Science Publishers, Amsterdam.
Luzzati, V., Gulik, A., DeRosa, M., & Gambacorta, A. (1987) *Chem. Scr. 27B*, 211–219.
Luzzati, V., Mariani, P., & Delacroix, H. (1988) *Makromol. Chem., Macromol. Symp. 15*, 1–17.
Macala, L. J., Yu, R. K., & Ando, S. (1983) *J. Lipid Res. 24*, 1243–1250.
Mariani, P., Luzzati, V., & Delacroix, H. (1988) *J. Mol. Biol. 204*, 165–189.
Nichols, B. W. (1963) *Biochim. Biophys. Acta 70*, 417–422.
Patton, J. S. (1981) *Physiology of the Gastrintestinal Tract* (Johnson, L. J., Ed.) pp 1123–1146, Raven Press, New York, NY.
Rivas, E., & Luzzati, V. (1969) *J. Mol. Biol. 41*, 261–275.
Rouser, G., Fleischer, S., & Yamamoto, A. (1970) *Lipids 5*, 494–496.

Seddon, J. (1990) *Biochim. Biophys. Acta 1031*, 1-69.
Shipley, G. G. (1973) *Biological Membranes* (Chapman, D., Ed.) Vol. 2, pp 1-89, Academic Press, London and New York.
Small, D. M. (1986) *The Physical Chemistry of Lipids from Alkanes to Phospholipids*, Plenum Press, New York and London.
Tardieu, A. (1972) Thesis, Université Paris-Sud.
Varskovsky, V. E., & Kostetsky, E. Y. (1968) *J. Lipid Res. 9*, 396.

The Formation of Cytochrome P-450 from Cytochrome P-420 Is Promoted by Spermine†

Gaston Hui Bon Hoa,*,‡ Carmelo Di Primo,‡ Marc Geze,‡ Pierre Douzou,‡ Jack A. Kornblatt,§ and Stephen G. Sligar‖

U310, INSERM, Service de Biospectroscopy, Institut de Biologie Physico-Chimique, 13, rue Pierre et Marie Curie, 75005 Paris, France, Enzyme Research Group, Department of Biology, Concordia University, Montreal H3G 1M8, Canada, and Department of Biochemistry, University of Illinois, Urbana, Illinois 61801

Received June 14, 1989; Revised Manuscript Received March 20, 1990

ABSTRACT: This paper is concerned with camphor-bound bacterial cytochrome P-450 and processes that alter its spin-state equilibrium and influence its transition to the nonactive form, cytochrome P-420, as well as its renaturation to the native camphor-bound cytochrome P-450. Spermine, a polycation carrying a charge of 4+, and potassium, a monovalent cation, were shown to differently cause an increase of high-spin content of camphor-bound cytochrome P-450. The spermine-induced spin transition saturates around 75% of the high spin; a further addition of KCl to the spermine-containing sample shifted the spin state to 95% of the high spin. The volume change of these spin transitions as measured by the use of high pressure indicated an excess of −40 mL/mol for the sample containing potassium as compared to that containing spermine. These results suggest that the proposed privileged site for potassium has not been occupied by spermine and that pressure forces both the camphor and the potassium ion from its sites, allowing solvent movement into the protein as well as ordering of solvent by the excluded camphor and potassium. Cytochrome P-420 was produced from cytochrome P-450 by hydrostatic pressure in the presence of potassium, spermine, and cysteine. Potassium cation shows a bigger effect on the stability of cytochrome P-450 than spermine or cysteine, as revealed by a higher value of the pressure of half-inactivation, $P_{1/2}$, and a bigger inactivation volume change. However, potassium cation did not promote renaturation of cytochrome P-420 to cytochrome P-450 while the presence of spermine did. The rate of renaturation to cytochrome P-450 was compared with that induced by cysteine, the only previously known effector of P-420 to P-450 interconversion. A probable electrostatic binding site for spermine is suggested and discussed.

Cytochrome P-450[1] is a monooxygenase that catalyzes the formation of 5-*exo*-hydroxycamphor from camphor, reduced putidaredoxin, and oxygen (Bradshaw et al., 1959; Hedegaard & Gunsalus, 1965). It has been shown that the overall electron-transfer and oxygenase activity of the enzyme is related to the percentage of the enzyme that is present as the high-spin form (Schwarze et al., 1985; Backes et al., 1982; Fisher & Sligar, 1985). The spin state of the substrate-bound enzyme is greatly modulated by cations, the most potent of which is potassium (Lange & Debey, 1979; Lange et al., 1979a, 1980). Sodium and spermidine also cause a shift of the high-spin state, but to a lesser extent, and appear to obey a general ionic strength dependence consistent with electrostatic shielding (Lange et al., 1979b). From the high-resolution X-ray structure of the substrate-bound and free enzyme, a cation binding site has been suggested to be located near the carboxy terminus of helix B′ (residues 86–96) with the cation coordinated to the amide carbonyls of glutamic acid-84 and tyrosine-96 (Poulos et al., 1987). Recent results using site-directed mutagenesis support this model (Di Primo et al., 1990).

The spin state of cytochrome P-450 with camphor bound is known to be influenced by pressure (Hui Bon Hoa & Marden, 1982; Marden & Hui Bon Hoa, 1982); this results from the pressure-induced displacement of the substrate camphor from the heme pocket (Fisher et al., 1985; Marden & Hui Bon Hoa, 1987). The resulting influx of water (Poulos et al., 1985, 1986; Fisher & Sligar, 1987) allows solvent coordination to the heme iron, thereby increasing the ligand field, favoring a low-spin, hexacoordinate configuration (Fisher & Sligar, 1985; Raag & Poulos, 1989). This solvation of the pocket is responsible for the spin-state change and a 170-mV shift in the redox potential (Sligar, 1976; Sligar & Gunsalus, 1976).

† This work was supported by INSERM (Unité 310), by Contract 85.T.0717 from MRT (France), and by NSERC (Canada). S.G.S. received a Fulbright Foundation Research Scholarship from the Commission Franco-Americaine.

‡ Institut de Biologie Physico-Chimique.
§ Concordia University.
‖ University of Illinois.

[1] Abbreviations: P-450, bacterial cytochrome P-450 involved in camphor hydroxylation; spermine, *N*,*N*′-bis(3-aminopropyl)-1,4-butanediamine.

0006-2960/90/0429-6810$02.50/0